Crystal chemistry of the solid solutions based on β-Mn

Jean-Marc Joubert, Jean-Claude Crivello

Crystal chemistry of the solid solutions based on β-Mn

Jean-Marc Joubert[1*], Jean-Claude Crivello[1,2]

[1]Univ Paris Est Creteil, CNRS, ICMPE, UMR 7182, 2 rue Henri Dunant, 94320 Thiais, France

[2]CNRS-Saint-Gobain-NIMS, IRL 3629, Laboratory for Innovative Key Materials and Structures (LINK), 1-1 Namiki, 305-0044 Tsukuba, Japan

[*]Corresponding author: jean-marc.joubert@cnrs.fr

Abstract

Binary solid solutions based on β-Mn have been systematically investigated from a structural point of view. The site occupancies of the substitutional solute elements Al, Co, Fe, In, Ir, Ni, Os, Ru, Si, Sn and Zn on the two distinct sites of its crystal structure have been determined experimentally by Rietveld refinement of X-ray or neutron powder diffraction data. The atomic distribution is discussed in light of the changes of lattice parameters in the solution and compared between the different chemical systems. A systematic analysis of the volume change within the complete binary systems has been carried out. Anomalies are observed and explained for the time, by assuming that Mn presents two different atomic radii at its two different sites. This feature is unique in metallic solid solutions in the absence of any mixed valence. The study is complemented by a detailed DFT investigation of the different systems demonstrating an anomaly with the description of the Mn atom by traditional first-principles calculations. This problem leads to miscalculation of the lattice parameter of pure Mn and, as a consequence, of the site occupancies in the binary systems. The importance of the ordering of the solute element for the Calphad modeling is discussed and the use of a two sublattice model for the description of β-Mn solid solutions in agreement with the presence of two different Wyckoff positions, instead of the conventional disordered solution model, is highly recommended.

Keywords: β-Mn, Rietveld, Calphad, site occupancies, DFT

1. Introduction

Among transition metals, Mn is unique. Firstly, it is the element with the most allotropic forms. Secondly, two of them, α- and β-Mn, are unique crystal structures that are not found as stable structures for any other element. They are complex structures compared to the classical transition metal structures *bcc*, *hcp* and *fcc* and are characterized by the presence of different non-equivalent sites which is rather unusual for pure elements.

The α-Mn structure (*A*12, *cI*58) [1, 2] is a pseudo-Frank-Kasper or topologically close packed (TCP) phase with 4 different sites in the space group $I\bar{4}3m$ (217). This structure also exists as the structure of intermetallic compounds. It is then known as the $Mg_{17}Al_{12}$ or Ti_5Re_{24} structure type depending on the state of order or as the χ phase, and exists in Al–Mg and in many rare earth–Mg and Re based systems.

The β-Mn structure (*A*13, *cP*20) [3] possesses 2 different sites in space group $P4_132$ (213), as shown in Fig. 1. The coordination polyhedron around site 8*c* (*x*=0.0635,*x*,*x*) is an icosahedron

(coordination number (CN) 12). That around site 12*d* (1/8, *y*=0.202, *y*+1/4) has CN14 and is also a Frank-Kasper polyhedron. The structure can therefore be considered as a TCP phase. The crystal structure may be interpreted in different ways summarized in Ref. [4] and has been related to the *C*15 structure [5]. It is a chiral structure. For a discussion on the determination of the absolute structure, see Ref. [6]. In the following, since only powder diffraction results will be discussed, chirality is not considered. The same structure is adopted by several binary intermetallic compounds where the two elements occupy the two different sites in a completely (Mg_3Ru_2 [7]) or partially (Au_9Nb_{11} [8], $Co_{2.5}Zn_{2.5}$ [5], $Cu_{0.815}Si_{0.185}$ [9]) ordered manner. In other systems, the state of order is unknown (Ag–Al, Al–Au, Fe–Mo, Fe–Re, Ga–V). Ternary derivatives such as Co–Mn–Zn compounds are skyrmion-host materials [10]. An ordered variant is known in which site 8*c* is split into two different 4*a* sites of space group $P2_13$, which are occupied differently. The structure type is then $AlAu_4$ [11] and the phase exists in Al–Au and Al–Cu systems. A filled variant known as π nitride or carbide also exists in many systems (sulfides, borides and phosphides are also reported) [12-15]. The prototype is then Mo_3Al_2C. The interstitial element is placed in a pseudo-octahedral site. All π compounds are purely ternary compounds. They neither originate from pure Mn nor from a known binary β-Mn compound by filling the interstitial site.

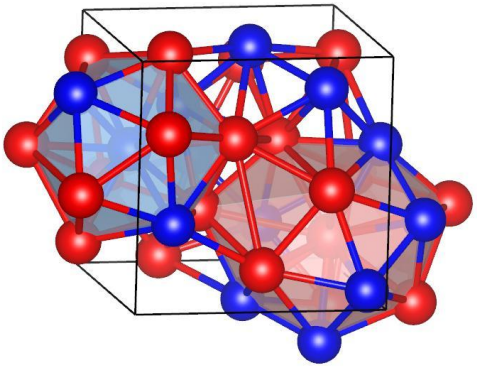

Figure 1: β-Mn crystal structure. The two sites 8*c* (blue) and 12*d* (red) are indicated with their respective coordination polyhedron CN12 (blue) and CN14 (red).

The transition between the α- and β-Mn has been well studied [16]. There is no obvious relationship between the structures. However, the diffraction patterns of the two structures are somewhat similar with the main peaks of α-Mn and β-Mn being very close to each other. This is because a_α is very near to $\sqrt{2}\ a_\beta$. This seems to be only a coincidence related to the fact that the ratio of the number of atoms per cell between the two structures (58/20) is close to $(\sqrt{2})^3$.

It should be noted that it is difficult to retain the β structure of pure Mn by quenching. This becomes much easier for solid solutions where the solute seems to stabilize the structure. While pure α-Mn orders antiferromagnetically at 95 K [17], β-Mn does not [18]. However, small amounts of alloying elements may induce the onset of magnetic ordering [19-24]. According to Drain *et al.* [25], pure β-Mn is a spin-liquid that transforms into a spin-glass with substitution. According to the same authors, the calculated ground state is ferrimagnetic. The study of the magnetic properties of β-Mn solid solutions is therefore quite interesting.

The similarity of α and β with intermetallic structures has led to them being referred to in the literature as 'single element' or 'self' intermetallic compounds. Though uncommon structures, they possess extended solubility ranges in many different binary systems as shown in Fig. 2 which also makes them attractive.

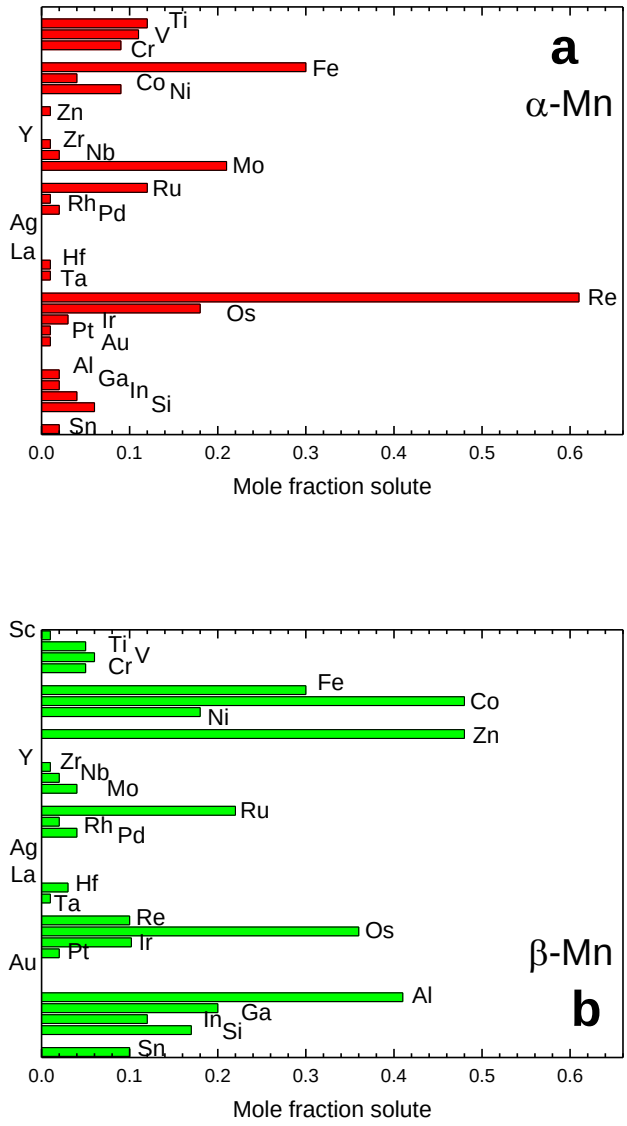

Figure 2: Maximum solubility in (a) α- and (b) β-Mn phases of transition metals and several *p*-elements as implied by the current versions of the phase diagrams [26] (Refs. [27] for Ir–Mn and [24] for Mn–Os systems).

Depending on the system, one may observe that the solubility may be large in α (Mn–Re), large in β (Al–Mn) or large in both phases (Fe–Mn). The magnitude of this solubility and the availability of different sites for the substitution make it important to determine the location of the solute through the measurement of the site occupancies. This is relevant in the framework of a general understanding of substitutional defect mechanism in TCP phases (see e.g., Ref. [28] for the σ phase and Ref. [2] for the χ phase). This is also critical in the framework of the Calphad modeling of such phases which are typical examples of terminal substitutional solid solutions with multiple sublattices [29]. The site occupancies in α-Mn have already been studied experimentally and reviewed in Ref. [2]. In the present work, we review the knowledge on the β-Mn phase, bring new experimental determination of site occupancies in many different systems using X-ray and neutron

diffraction. To complete the study, we will also present first principles calculations in the frame of the density functional theory (DFT) to study atomic volumes, phase stability and site occupancies.

2. Experimental details

All the samples were synthesized by powder metallurgy. Mn powder was obtained by crushing Mn flakes recently washed with hydrochloric solution. For the other elements, commercial powders were used (for details see Table 1). In each case, a pellet (6 mm diameter) was obtained and pressed to 2 tons. Reaction treatment in argon backfilled silica tubes was chosen according to the known phase diagrams [30] or the literature in the specific cases of Ir–Mn [27] and Mn–Os [24]. After the thermal treatment, the samples were analyzed by Electron Probe Microanalysis (EPMA).

Table 1: Source and characteristics of the raw materials used for the synthesis.

Element	Provider	Purity (%)	Grain size
Mn	Alfa Aesar	99.95	pieces reduced into powder (<100 µm) before preparation
Al	Alfa Aesar	99.97	<44 µm
Co	Aldrich	99.9	<150 µm
Fe	Alfa Aesar	99.9	<74 µm
In	Alfa Aesar	99.99	<44 µm
Ir	Chempur	99.9	<44 µm
Ni	Alfa Aesar	99.996	<125 µm
Os	Aldrich chemical	99.9	<44 µm
Ru	Chempur	99.9	<60 µm
Si	Alfa Aesar	99.9985	<20 µm
Sn	Baudier	99.9	<44 µm
Zn	Ceras	99.999	<44 µm

X-ray diffraction (XRD) was used to characterize the samples. Samples were easily reduced to powder and were measured using Cu Kα radiation and the Bragg-Brentano geometry. The diffractometer is equipped with a graphite monochromator in the diffracted beam. The Rietveld method was used to analyze the XRD data. Internal coordinates, isotropic displacement parameters, and site occupancies were refined. The refinement of the displacement parameters is always affected by the micro-absorption phenomenon. They are therefore not reported. Site occupancies were refined assuming the complete occupancy of both sites (no vacancy) and a global composition matching the analyzed (EPMA) composition. Thus, only the distribution of a given amount of the solute on the two sites was refined corresponding to the refinement of a single parameter.

Neutron diffraction was used for the solute elements without X-ray diffraction contrast (atomic number close to that of Mn: Co, Fe, Ni, Zn). The samples (powder, ~5 g) were contained in a vanadium can (diameter 5 or 8 mm). The measurement was performed at the ILL on D1B diffractometer in Debye-Scherrer geometry (λ=1.29 Å, 2θ range 1-129°). The data analysis was very similar to that used for the X-ray results. Absorption correction was taken into account. In several cases, the negative scattering factor of Mn exactly compensates that of *X* at one or the other site. In this case, the position and the displacement parameter for this site was fixed to the X-ray data. In one case, $Mn_{0.72}Fe_{0.28}$, the scattering factors of Mn (-3.7 fm) and iron (9.45 fm) almost compensate for the overall composition. Though a nice diffraction pattern was obtained (which testifies the order

between the two sites), it is impossible to conduct the refinement of the site occupancies since any distribution of atoms gives roughly the same intensity ratios between the peaks.

3. Calculation details

The DFT method has been used to perform the electronic structure calculations [31, 32]. The Projector Augmented Wave (PAW) pseudo-potentials method was used as implemented in the VASP Package with a 600 eV cutoff energy [33-36] (VASP 6.2 version using PAW POTCAR files: PBE version 54, with the standard state, such as Mn with 7 electrons). After several tests using different functionals (LDA or PBE-sol [37]), the exchange and correlations were considered in the Generalized Gradient Approximation (GGA) with the Perdew-Burke-Ernzerhof (PBE) functional [38, 39]. Calculations with collinear spin polarization were considered. Both the lattice parameters and internal atomic coordinates were fully relaxed by several intermediate steps, so that the self-consistent total energy calculations converged to less than 0.01 meV. The final energies were calculated using the linear tetrahedron method with Blöchl corrections [40]. The Monkhorst-Pack procedure was used to generate 220 points in the irreducible wedge of the Brillouin zone, from a 19x19x19 k-points meshing [41]. The charge distribution on the atoms was investigated using Bader's topological analysis [42], using the code developed by Henkelman *et al.* [43].

Since the β-Mn phase is composed of two nonequivalent 8*c* and 12*d* sites, four ordered configurations can be calculated for a binary Mn–*X* system: Mn_8Mn_{12}, X_8Mn_{12}, Mn_8X_{12}, X_8X_{12}. These four compounds were calculated systematically for a set of 11 Mn-*X* binaries, with *X* =Al, Co, Fe, In, Ir, Ni, Os, Ru, Si, Sn, Zn. In addition, the dilute solutions $Mn_{19}X_1$ with distributions of *X* either in 8*c* and 12*d* were also considered. The heat of formation of each configuration is given by the difference of its total DFT energy with respect to the element energies in their stable reference state (SER).

In addition to this systematic investigation of the β-Mn phase, *X* pure elements and about 40 Mn–*X* intermetallic compounds with different crystal structures were also calculated under the same conditions.

4. Results

4.1. DFT calculations

All the results are given in Table S1 of Supplementary Material. The ground state of each system is plotted in Fig. S1.

Analyzing the ground state of the β-Mn phase for each system i.e., the relative position of the configurations X_8Mn_{12} and Mn_8X_{12} compared to the pure elements in the β-Mn structure, one may easily distinguish four possible cases.

- none of the binary configurations is stable (*X*=Co, In, Sn)
- X_8Mn_{12} only is stable (no system)
- Mn_8X_{12} only is stable (*X*=Al, Ir, Ni, Os, Ru, Zn)
- both configurations are stable (*X*=Fe, Si)

For the third group, the solute *X* prefers site 12*d*, the higher CN14 site. For the fourth group, the solute *X* prefers site 8*c*, the smaller CN12 site, at least for *X* concentration lower than 0.4. For the first group, it is more difficult to establish site preference, and one has to look at the relative energies

of the diluted structures Mn_7XMn_{12} and $Mn_8Mn_{11}X$. In each case the second arrangement is found to be more stable indicating the preference for the site with CN14.

The electronic charge transfers support this discussion of site preference. They have been calculated using Bader's theory. This method looks for the cancellation of the squared wave function gradient in direct space and integrates the electron in the corresponding sphere. Well used for the description of molecular bonds in organic chemistry, the approach is more limited for metallic bonds, with a known poor estimation of the Bader radii and charges but giving the general trends by relative comparison. According to Table S1, the corresponding properties vary as a function of the distribution of atoms along their site. Pure Mn shows an electronic charge transfer from the site 12*d* to 8*c* (about 0.1 e-), which leads to a better localization of the 3*d* orbitals in 8*c* and thus to a smaller Bader radius in site 8*c* than in site 12*d*. This trend is similar for other pure elements where 8*c* is always negatively charged with an associated smaller radius, except for Si which differs from the other *d*-electrons elements because of its *s*-*p* characters. In the binary compounds, it is interesting to note that the ground state compounds show also an anionic preference for valence electron rich atoms in the site 8*c*. This is in agreement with the discussion in Ref. [44] suggesting that the majority components are cationic in nature because of nearest neighbor distance criterion.

The atomic volume calculated by DFT for pure Mn (10.7 $Å^3$ for α, 10.8 $Å^3$ for β) is much smaller than the experimental one (12.2 $Å^3$ for α, 12.6 $Å^3$ for β). To help understanding this anomaly, we systematically calculated the atomic volume of 40 different intermetallic phases in various Mn–*X* systems (*X* = Al, Co, Fe, In, Ir, Ni, Os, Ru, Si, Sn, Zn) by DFT (in PBE, at 400 eV and 800 eV cutoffs). The relative difference between the DFT volume and the experimental one is shown in Fig. S2 as a function of *X* content. It shows that the volume of Mn-based intermetallic compounds, whatever the crystal structure, is systematically underestimated and that the deviation is proportional to the Mn concentration. It is shown that the volume of α- and β-Mn underestimated by DFT is neither related to any particular feature of these two structures nor to the magnetic contribution (since the deviation occurs also with *X* elements that are not magnetic), but rather related to the presence (and proportional to the amount) of Mn itself as an element.

4.2. Experimental results

The synthesis was successful for all samples and homogeneous β single-phase samples were generally obtained. The quenching was efficient to stabilize the β phase and the samples are therefore considered to be in the equilibrium state at the temperature they have been prepared. Only in few cases, secondary phases were observed by diffraction but always in a small amount. Additionally, in some cases traces of MnO were noticed by neutron diffraction technique in which this phase is more visible, but never in a quantity such that it could affect the composition of the β-Mn phase which is, anyhow, checked by EPMA. Examples of X-ray and neutron diffraction diagrams are presented in Fig. 3 in the form of conventional Rietveld plots. The results are presented in Table 2 including the EPMA and results from the Rietveld analysis (lattice parameters, internal coordinates and site occupancies).

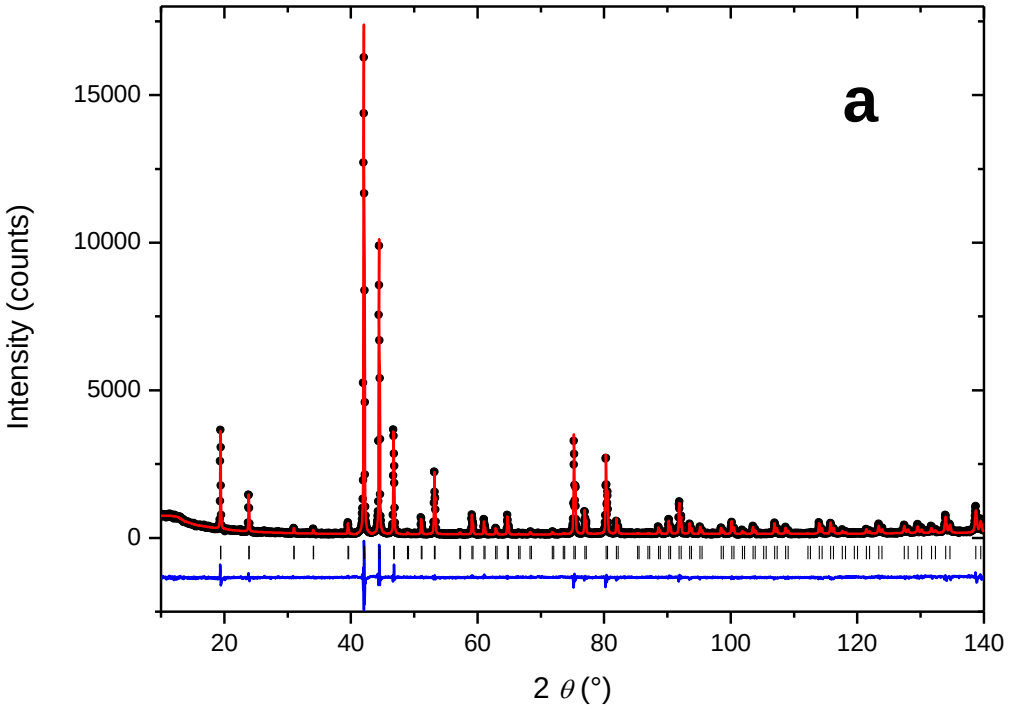
a
Intensity (counts)
15000
10000
5000
0
20
40
60
80
100
120
140
2 θ (°)

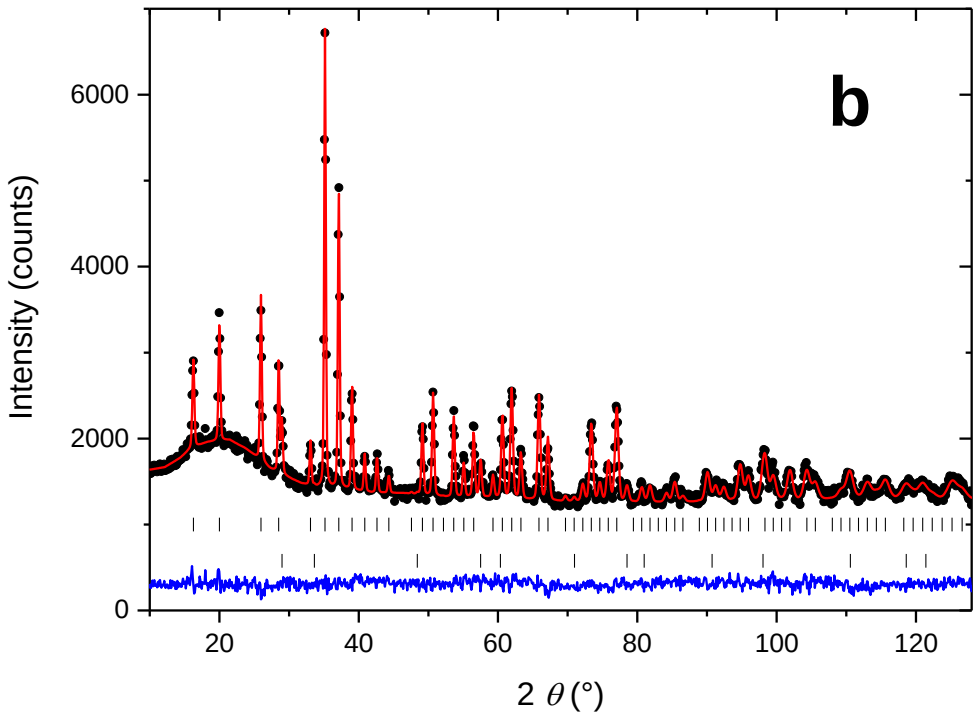
b
Intensity (counts)
6000
4000
2000
0
20
40
60
80
100
120
2 θ (°)

Figure 3: Rietveld plot of (a) $Mn_{0.6}Al_{0.4}$ (X-ray) and $Mn_{0.88}Ni_{0.12}$ (neutron). Experimental (points), calculated (line) and difference (line below) patterns are shown. The markers show the positions of the diffraction lines. The second phase in (b) is MnO.

Table 2: Sample nominal composition, heat treatment, analyzed composition from EPMA, lattice parameter and internal coordinates from XRD, site occupancies (in atom per site i.e., ranging from 0 to 8 or 0 to 12, * indicates neutron results), remarks. Typical estimated standard deviations for lattice parameters are 0.0001 Å and 0.0003 for internal coordinates.

Composition	Heat treatment	Analyzed composition	*a* (Å)	*x*	*y*	Occupancy 8*c* (atom)	Occupancy 12*d* (atom)	Remarks, presence of additional phases
$Mn_{0.9}Al_{0.1}$	870°C, 14 days	$Mn_{0.919(4)}Al_{0.081(4)}$	6.3485	0.0644	0.2026	-0.05(6)	1.67(6)	
$Mn_{0.8}Al_{0.2}$	870°C, 14 days	$Mn_{0.808(4)}Al_{0.192(4)}$	6.3823	0.0660	0.2033	-0.02(5)	3.86(5)	
$Mn_{0.7}Al_{0.3}$	870°C, 14 days	$Mn_{0.734(4)}Al_{0.266(4)}$	6.4046	0.0672	0.2038	-0.20(3)	5.52(3)	
$Mn_{0.6}Al_{0.4}$	870°C, 14 days	$Mn_{0.641(4)}Al_{0.359(4)}$	6.4256	0.0681	0.2045	-0.08(4)	7.26(4)	
$Mn_{0.8}Co_{0.2}$	900°C, 14 days	$Mn_{0.786(2)}Co_{0.214(2)}$	6.3192	0.0638	0.2017	3.64(5)*	0.64(5)*	
$Mn_{0.6}Co_{0.4}$	900°C, 14 days	$Mn_{0.599(1)}Co_{0.401(1)}$	6.2850	0.0623	0.2008	6.33(7)*	1.69(7)*	
$Mn_{0.85}Fe_{0.15}$	850°C, 14 days	$Mn_{0.850(2)}Fe_{0.150(2)}$	6.2951	0.0632	0.2021	2.40(2)*	0.60(2)*	
$Mn_{0.72}Fe_{0.28}$	850°C, 14 days	$Mn_{0.695(4)}Fe_{0.305(4)}$	6.2727	0.0631	0.2027			site occupancies cannot be refined
$Mn_{0.9}In_{0.1}$	870°C, 14 days	$Mn_{0.9055(5)}In_{0.0945(5)}$	6.5190	0.0672	0.2040	0.05(4)	1.84(4)	
$Mn_{0.9}Ir_{0.1}$	850°C, 14 days	$Mn_{0.918(3)}Ir_{0.082(3)}$	6.4508	0.0646	0.2025	1.54(2)	0.10(2)	
$Mn_{0.88}Ni_{0.12}$	750°C, 14 days	$Mn_{0.876(2)}Ni_{0.124(2)}$	6.3615	0.0631	0.2022	2.09(1)*	0.39(1)*	MnO in the neutron pattern
$Mn_{0.85}Os_{0.15}$	950°C, 14 days	$Mn_{0.862(2)}Os_{0.138(2)}$	6.4619	0.0639	0.2031	2.52(2)	0.24(2)	
$Mn_{0.7}Os_{0.3}$	950°C, 14 days	$Mn_{0.700(4)}Os_{0.300(4)}$	6.5687	0.0643	0.2037	5.22(3)	0.78(3)	*hcp* phase
$Mn_{0.55}Os_{0.45}$	950°C, 14 days	$Mn_{0.55(1)}Os_{0.45(1)}$	6.5711	0.0647	0.2044	7.84(9)	1.16(9)	*hcp* phase
$Mn_{0.9}Ru_{0.1}$	750°C, 14 days	$Mn_{0.894(3)}Ru_{0.106(3)}$	6.4124	0.0638	0.2023	1.60(3)	0.52(3)	MnO and α-Mn
$Mn_{0.8}Ru_{0.2}$	750°C, 14 days	$Mn_{0.751(9)}Ru_{0.249(9)}$	6.4916	0.0648	0.2032	3.75(5)	1.23(5)	
$Mn_{0.88}Si_{0.12}$	900°C, 14 days	$Mn_{0.883(1)}Si_{0.117(1)}$	6.2727	0.0604	0.1988	2.2(1)	0.1(1)	
$Mn_{0.9}Sn_{0.1}$	870°C, 14 days	$Mn_{0.904(1)}Sn_{0.096(1)}$	6.5091	0.0667	0.2036	0.02(3)	1.90(3)	Mn_3Sn and MnO
$Mn_{0.8}Zn_{0.2}$	850°C, 10 days							
	500°C, 10 days	$Mn_{0.860(2)}Zn_{0.140(2)}$	6.4050	0.0654	0.2038	-0.02(2)*	2.82(2)*	α-Mn (and MnO in the neutron pattern)

Lattice parameters as a function of solute composition are plotted in Fig. 4. They emphasize the increase (or decrease) of the lattice parameters generated by the substitution. The same plot is presented in Fig. S3 with a comparison of the available literature. Additionally, for each system a complete atomic volume plot function of the composition including all the phases is presented in Figs. S4. This plots also contain the DFT volumes for the β phase.

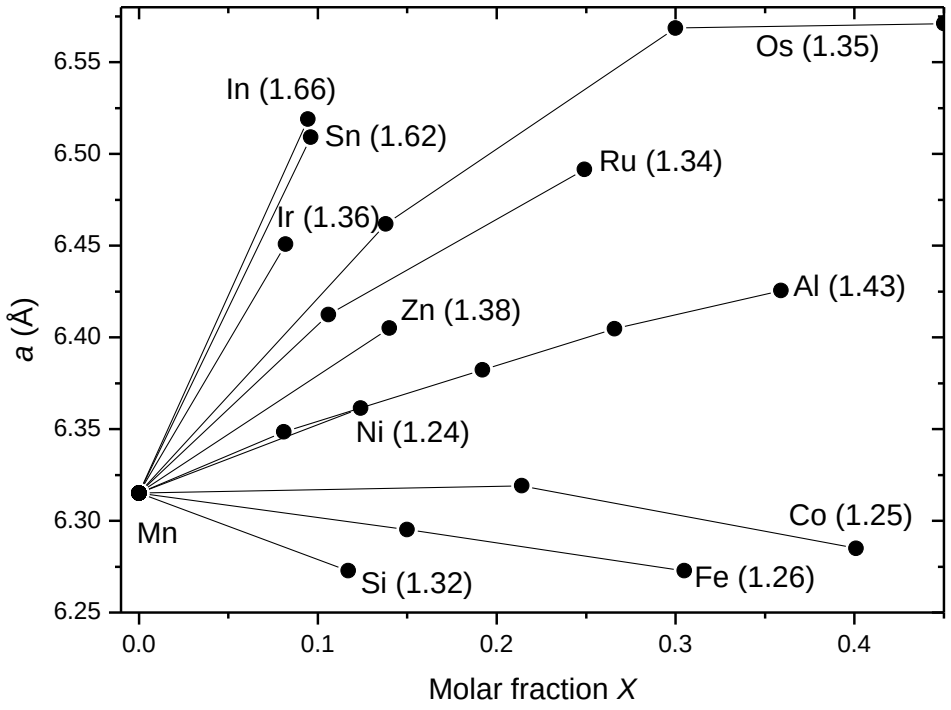

Figure 4: Lattice parameter as a function of the solute composition. Atomic radii are shown in brackets.

The evolution of the lattice parameters is generally linear for the system in which several compositions have been measured, in the composition range that has been investigated. As usual for solid solutions, the slope should be related to the radius of the solute element. However, several elements (Ir, Ni, Os and Ru) increase the lattice parameters much more than expected from their atomic radius. For example, Ni, in principle smaller than Mn, increases the lattice parameter, and this as much as Al which is obviously much larger than Ni. At this point we may mention that the atomic radius of Mn itself (in principle 1.35 Å) is still a matter of controversy (see e.g., the discussion in Refs. [2, 28]). In these two works, an atomic radius around r_{Mn} = 1.30 Å was extrapolated.

The atomic coordinates x_{8c} and y_{12d} plotted in Fig. S5 show a linear evolution as a function of the composition. The slope is related to the atomic radius of the solute, more strictly than the lattice parameter itself. A plot of y_{12d} as a function of x_{8c} is also shown.

Site occupancies, plotted in Fig. 5, are very well rationalized by considering two types of *X* solute elements. Several elements occupy exclusively site 12*d* while the other elements strongly prefer site 8*c* but also have a small occupancy on site 12*d*. Contrary to what is observed for the lattice parameters, the site preference is clearly determined according to the atomic radius of the

solute element. Elements with atomic radius smaller than 1.37 Å (Co, Fe, Ir, Ni, Os, Ru, Si) occupy low CN site 8*c*, preferentially. Elements with atomic radius larger than 1.37 Å (Al, In, Sn, Zn) occupy high CN site 12*d*, exclusively. The limit of 1.37 Å does not correspond to the radius of Mn. Ir, Os and Ru are clearly larger than Mn and occupy nevertheless the sites of smaller CN. Electronic criterion better justifies the distribution of the elements. The *d* elements with more valence electrons than Mn occupy sites of lower CN (but no element with less valence electron has a solubility higher than 5 at.%) while more electropositive *p* elements (excepting Si) occupy the sites with high CN.

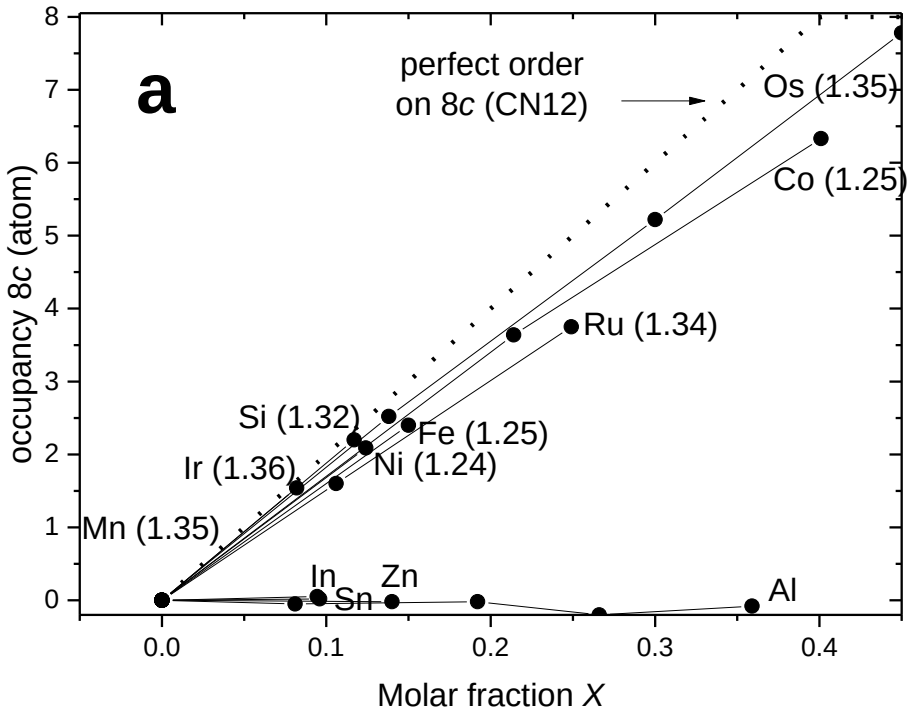

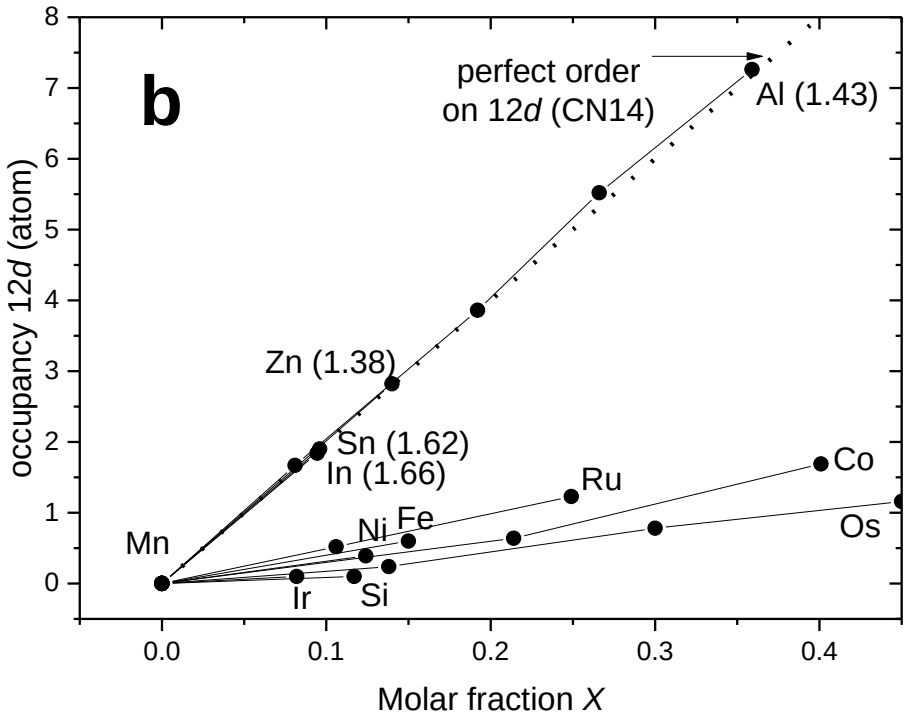

Figure 5: Site occupancies (in atom per site) on sites (a) 8*c* and (b) 12*d* as a function of the solute composition.

This very clear ordering between one or the other site is similar to that observed in the α-Mn structure [2] but contrasts with what is observed in other TCP phases such as the σ phase in which mixing in several sites at the same time is almost always the rule [28].

5. Discussion

5.1. Synthesis

The sample synthesis using powder metallurgy was successful. In the literature, mainly arc melting was used, also successfully. However, we believe that, given the high vapor pressure of manganese at the melting temperatures of the different elements, powder metallurgy allows a better control of the composition and the synthesis of alloys with refractory elements (Os…). This technique was also successfully used previously in the synthesis of α-Mn samples in particular with Re and Ru [2]. It also prevents segregation during the solidification. It seems that diffusion is sufficiently fast at the chosen temperatures corresponding to the stability of the β-Mn phase (around 1000°C) to warrant a complete reaction between grains with sizes ~40 µm.

5.2. Comparison with literature

A review of the literature data on β-Mn solutions is given in Table 3. The type of data indicated in the different references is provided. Other publications are not mentioned in the Table 3, mainly because they address the magnetic properties of several systems at the same time [19, 23, 45-48]. It is evident that the main focus of all the previous literature on β-Mn solutions was the study of the magnetic properties, or better said, of the changes of the magnetic properties of pure β-Mn [49, 50] with the solute nature, and sometimes concentration.

Table 3. Literature data on β-Mn solutions. Lattice parameters are reported in most publications.

Solute	Reference	Type of data
Al	[51]	Site occupancies (X-ray diffraction), magnetic properties
	[52]	Magnetic properties
	[53]	Magnetic properties
	[54]	Magnetic structure, site preference (neutron diffraction)
Co	[20]	Magnetic properties
	[55]	Site occupancies (neutron diffraction)
	[56]	Site occupancies (neutron diffraction), magnetic properties
	[57]	Magnetic properties, magnetic structure, site preference (neutron diffraction)
Fe	[58]	Site preference (Mössbauer), magnetic properties
	[22]	Site preference (Mössbauer)
	[59]	Site preference (Mössbauer)
	[55]	Site occupancies (neutron diffraction)
	[60]	Site preference (Mössbauer), magnetic properties
Ge*	[21]	Magnetic properties
In	[61]	Site preference (neutron diffraction), magnetic properties
Ir	[27]	Site preference (X-ray diffraction), magnetic properties
Ni	[55]	Site occupancies (neutron diffraction)
Os	[24]	Phase diagram, magnetic properties, site occupancies
	[62]	Specific heat, magnetic properties
	[63]	Magnetic properties
	[64]	Magnetic properties
Ru	[65]	Site preference (X-ray diffraction), magnetic properties
	[66]	Magnetic properties
	[67]	Magnetic properties
	[68]	Magnetic properties, magnetic structure
Sn	[69]	Site occupancies (Mössbauer), magnetic properties
	[70]	Site occupancies (Mössbauer, neutron diffraction)
	[22]	Site preference (Mössbauer)

* solute not studied in the present work

Lattice parameters in the solid solutions are generally well known and can be compared with our own results in Fig. S3 showing a good agreement. Several studies were devoted to the localization of the solute in the structure, in particular because of its influence on the magnetic properties. In general, only the qualitative site preference was obtained from the analysis of either Mössbauer or diffraction data. This was done mostly by comparison between the experimental data and models generated by a substitution on one or the other site. Intermediate cases in which the solute would be partitioned on the two sites were not considered in these studies. The study of the literature suggests that one should be very careful in analyzing the data, especially from Mössbauer spectroscopy. This is because many errors can be produced and completely inverse site occupancies

reported (see e.g., Ref. [59] contradicted by Ref. [55] for Fe with a re-analysis of the previous data, and Ref. [70] contradicted by Ref. [71] for Sn).

Only, in few cases, a real refinement of the data is provided allowing a quantitative determination, for a single composition: Al [51], Co [55], Fe [55], Ni [55], Sn [22, 69, 71]. A determination as a function of composition occurs in even fewer cases (Co [56]). In summary, in the literature only trends are given, qualitative site preference but rarely a quantitative analysis has been made and when it is the case, the refinement has not always been conducted in satisfactory conditions.

In the present work, for the first time, a systematic and comparative study is provided. It encompasses all the possible solutes having a substantial solubility. Our study is conducted as a function of composition when the homogeneity range is sufficiently large, and the refinements have been conducted using rigorous Rietveld analysis conducted in the same conditions for all the samples. When data is available, our results confirm the trends shown in the literature (see the comparison in Fig. S6), but subtle features such as the slight occupancy of site 12*d* by the atoms preferring site 8*c* are revealed in the present work.

5.3. Volume anomalies

An analysis of the atomic volume in all the systems we have studied as a function of composition is provided in Fig. S4. The plots allow us to put into perspective the volume of the β-Mn phase with the volume of all other phases. These plots were intended to find an explanation for the volume anomalies noticed previously in certain systems.

First, the volume of pure α (12.2 $Å^3$) and β-Mn (12.6 $Å^3$) should be considered. Both are very small, especially when compared with the volume that can be expected for pure Mn in the *fcc* structure (at room temperature), extrapolated from that of the *fcc* solid solutions in Fe–Mn, Ir–Mn and Mn–Ni systems (~13.2 $Å^3$). This would indicate either a very high compacity (around 80%) for these two structures compared to *fcc*, already known to be one of the most compact structures (compacity 74%), or the fact that Mn radius is different in these two structures. Both explanations can be considered.

A better compacity than *fcc* can be achieved only if one considers the packing of atoms with different sizes. This is actually the basic construction principle of TCP structures of which β-Mn is a representative. β-Mn structure has already been presented as a kind of self-intermetallic compound. One could therefore imagine that it is constituted by atoms with different sizes (‘large’ Mn and ‘small’ Mn). An analysis of the distance between sites of CN12 gives an atomic radius of 1.18 Å while that between the sites of CN14 gives an atomic radius of 1.32 Å supporting, at least qualitatively, this assumption. Note that this has been postulated also in Ref. [4]. This is also confirmed by the Bader radius obtained from the DFT calculations in β-Mn (1.36 for 8*c*-CN12 and 1.38 Å for 12*d*-CN14). The systematic study of the Bader charges of Mn alloyed with the *X* element also shows a clear electronic charge transfer from the site 12*d* to site 8*c* site, leading to a preference for a negative charge on site 8*c* and an associated smaller Bader volume, consistent with its small coordination associated with shortest nearest neighbor distances compared to 12*d* [44].

We consider now binary systems. When a solute substitutes Mn, one should not consider its atomic size compared to that of Mn but rather the size difference compared to the type (‘large’ or ‘small’) of Mn it replaces, depending on the site the solute occupies. For the elements preferring site

12*d* (CN14), the magnitude of the cell parameter increase as a function of composition follows a logical trend: larger atoms (In, Sn) have a larger effect than smaller atoms (Ga, Al, Zn). The weak lattice parameter increase of Al is explained by the small difference of atomic radius between Al and the 'large' Mn it replaces. A 'large' Mn apparent atomic radius of ~1.38 Å would explain most of the data.

For the elements preferring site 8*c* (CN12), the magnitude of the increase is also qualitatively reproduced: larger atoms (Ir, Ru, Os) have a larger effect than smaller atoms (Ni, Co, Fe, Si). The absence of a strong lattice parameter decrease for Co and Fe is explained by the small difference of atomic radius between these elements and the 'small' Mn it replaces. A 'small' Mn apparent atomic radius of ~1.25 Å would explain most of the data.

This explanation has the merit to explain why Ni with an evidently smaller atomic radius than Al increases as much the lattice parameter and why the expansion related to the solution of Ir, Ru and Os is so large.

For a complete substitution of Mn by an element having an atomic volume intermediate between the 'small' and the 'large' Mn radii, one would therefore expect, first, an increase of the volume when replacing the 'small' Mn on the CN12 site, up to the composition $Mn_{0.6}X_{0.4}$, for a perfectly ordered scheme, then a decrease when replacing the 'large' Mn on the CN14 site. By chance, Co has been observed as a metastable phase in the β-Mn structure after decomposition of an organo-metallic [72]. The plot of atomic volume for Co–Mn system in Fig. S7 perfectly fits the proposed model since a maximum is indeed observed for the β-Mn solid solution volume. The maximum is not located exactly at the composition $Mn_{0.6}Co_{0.4}$. This is explained by the fact that the substitution is not completely ordered, and that Co starts to replace Mn on the CN14 site before reaching the composition $Mn_{0.6}Co_{0.4}$.

5.4. DFT anomalies

The equilibrium volume calculated by DFT-PBE is extremely small (10.7 $Å^3$ for α, 10.8 $Å^3$ for β), even much smaller than the experimental one, already shown above to be very small. This is not the usual behavior for PBE which generally tends to overestimate the cell parameters. Similar volumes are obtained with LDA (10.1 $Å^3$ and 10.2 $Å^3$ for α and β respectively), PBE-sol functional (10.4 $Å^3$ and 10.5 $Å^3$) and even a meta-GGA using SCAN (10.5 Å). This behavior has already been noticed in the literature [18, 25], even using full potential method, but was not explained, as far as we are aware.

For α-Mn, a calculation with a cutoff larger than usual (800 eV) allows a better reproduction of the volume, but this is not the case for β-Mn. Many tries have been done with manual optimization, taking care of the non-colinear spin polarization, etc. and conclude than the PBE Mn potential has a weird behavior dealing with the β-Mn structure. Given that the pseudo or full potentials methods choice seems to have no impact on this outcome, the anomaly must be linked to an inherent issue with the semilocal type of approximation. This holds true regardless of the DFT package used. Consequently, a more sophisticated level of approximation for the exchange-correlation effects is necessary in the case of manganese.

To understand the discrepancy between calculated and experimental volumes, we performed systematic calculations of all the ordered compounds through the complete binary systems (see Fig. S2), including many non-magnetic elements. It is evident that the difference between calculated and experimental volumes gets larger as a function of the Mn concentration. The

discrepancy is therefore not related to the structure of β-Mn, as also shown by the DFT calculation of Mn in the *fcc* structure (10.7 Å^3) but rather to the element itself. This result also highlights the fact that this behavior is independent of the magnetic contribution, since the deviation is observed for high *X* concentrations, when *X* is a paramagnetic element and in cases when the DFT binary calculation converges to a non-magnetic state. This indicates a clear problem with the actual Mn pseudo-potential or, at least, with the semilocal (LDA, GGA, meta-GGA) type of approximation (regardless of which DFT package is used), such that a more advanced level of approximation for the exchange-correlation effects should be used in the case of Mn.

For the binary systems, we can compare the experimental site occupancies with the obtained site preference obtained from the DFT calculations. Except for Fe and Si, we found a systematic preference for the site of larger coordination. This is consistent with the observed site occupancies for Al, In, Sn and Zn, but not at all for Co, Ir, Ni, Os and Ru that prefer the site of smaller coordination.

All the Mn compounds, as we have shown previously, suffer from an underestimation of their atomic volume by DFT proportional to Mn composition. This would necessarily include the ordered configurations that we have calculated Mn_8X_{12} and X_8Mn_{12}. The plots in Figs. S4 show that the calculated volume of these two configurations is always far below that obtained from drawing a straight line between the experimental volume of pure Mn and the calculated volume of the configuration X_8X_{12} representing the element *X* in the structure of β-Mn, which is in reasonable agreement with the experimental volume for the element *X*. This volume reduction is due to the wrong DFT calculation of Mn compounds. But this imposes a strain on the *X* atom in the structure that may not have sufficient space. This would explain why this element would be more stable in the high CN configuration because it has more space to accommodate its atomic size. This may explain the wrong site preference obtained from DFT for the elements Co, Ir, Ni, Os and Ru.

To demonstrate this feature, calculations have been made for the Mn–Ni system with an expanded cell. Formation enthalpies relative to the pure elements in their standard state are plotted as a function of volume in Fig. 6. For volumes comparable to the expected experimental volume (above 12.5 Å^3/at.), the configuration Ni_8Mn_{12} starts to be stable over the configuration Mn_8Ni_{12}. Though the energies cannot be compared quantitatively (because one cannot compare the relative stability of different configurations at different compositions, and because it is difficult to guess at which volume should be taken each configuration), the plot is however very meaningful qualitatively. It explains how the wrong volume estimation affects the relative stability of the two binary

configurations as illustrated schematically in the inset of Fig. 6.

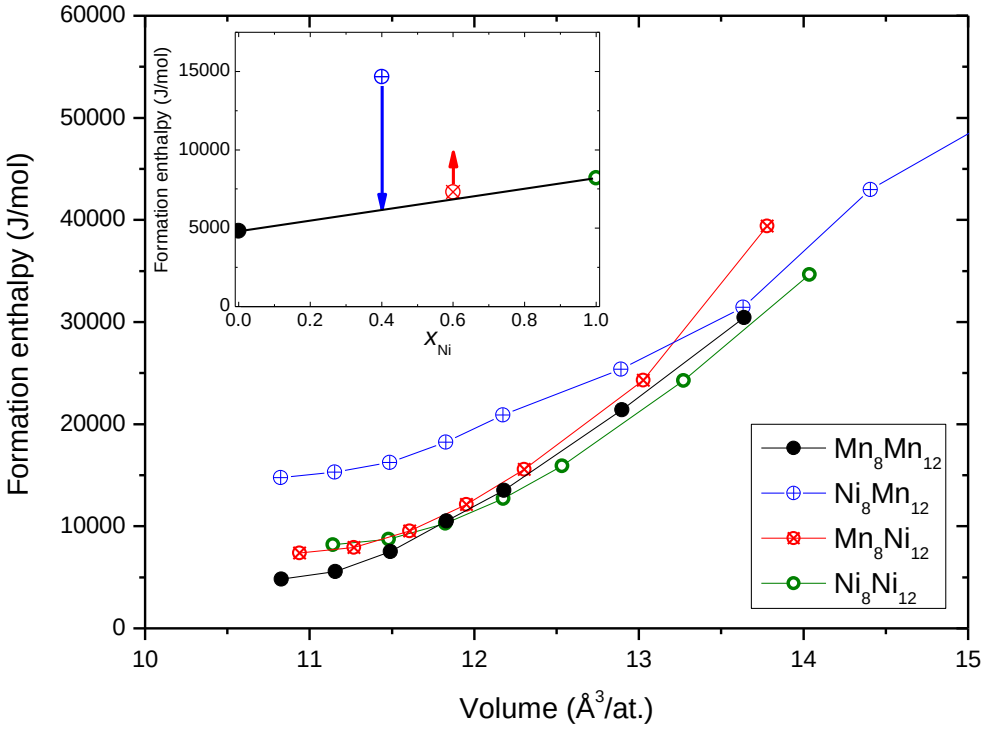

Figure 6: DFT enthalpies of formation (relative to the pure elements in their standard state) of the different ordered configurations in the Mn–Ni system as a function of the volume using PBE. The inset shows the relative effect of the dilatation, obtained by increasing the DFT volume, on the ground state.

5.5. Comparison between α- and β-Mn phases

Very few elements have a large solubility in both phases allowing a comparison. This is the case only for Fe and Ru. The site occupancies of these two elements in the two phases are compared in Fig. S8. It can be seen that similar trends are observed i.e., preferential occupancy of the low coordination sites (CN12, 24g_2 in α- and 8*c* in β-Mn phases). Of course, the situation is more complex in α-Mn structure because of a larger number of sites and the availability of a site of intermediate coordination (CN13). But, overall, the same trends are observed.

5.6. Calphad modeling

The behavior we observe here with a clear site preference and, therefore, a strong difference with a classical terminal solid solution behavior was anticipated in our previous work [29], especially because of the similarity with the α-Mn structure also studied in one of our previous works [2]. Both phases have the structure of intermetallic compounds. They should therefore be described as such i.e., using the sublattice model [73] rather than a disordered substitutional solid solution model consisting in imposing, from the thermodynamical point of view, the same site occupancy on both sites.

We propose to use a sublattice model $(Mn,X)_8(Mn,X)_{12}$. Such a model allows to respect and to take into account the experimental site occupancies. The difference on the calculated configurational entropy can be huge since our model orders at the composition Mn_8X_{12} or X_8Mn_{12} (zero mixing entropy) while the mixing entropy is almost maximum in a conventional single site substitutional model. This cannot be corrected using excess terms because the temperature dependence of the Gibbs energy is not the same. Not only the entropy, but also the enthalpy itself can be incorrectly calculated since the enthalpic contribution of the ordered compound can only be taken into account using interaction parameters. The shape of the enthalpy curve is therefore very different.

Another issue is the phase continuity, possible in some systems, with an intermetallic of the same structure. The system Co–Mn–Zn illustrates perfectly this problem [74]. As said in the introduction an intermetallic exists in the binary system Co–Zn with the same crystal structure as β-Mn. In the ternary system, this compound accepts a Mn solubility going all the way to the pure element (see Fig. 2 in Ref. [74]). While it would be logical to describe the binary compound with a sublattice model $(Co,Zn)_8(Co,Zn)_{12}$, as it is the rule, it may extend up to pure β-Mn only by using the same model that should therefore be also used for binary β-Mn solid solutions in Co–Mn and Mn–Zn system, and by extension to any system involving Mn. Note also that the site occupancies have been measured in this ternary system [10] and are in agreement with the results found for the binary Co–Mn and Mn–Zn.

As described in Ref. [29], note that the ordering discussed here differs from the ordering of conventional solid solutions since, in the present case, the different sites are already present in the pure element, the ordered dissolution of the solute occurs with the first atom, does not involve breaking of symmetry and change of the space group and there is no phase transition.

In particular, systems such as Fe–Mn [75] and Al–Fe–Mn [76-79] should be reoptimized in this context given both the technological importance of these systems and the extremely wide homogeneity range of the β-Mn solid solution. Note that the proposed model has been very recently used for the optimization Mn–Fe–Ti system [80, 81].

6. Conclusion

Solid solutions based on β-Mn have been studied in various binary systems. Cell volume dependence as a function of composition is anomalous and is explained by considering two different radii for Mn on the two sites of the crystal structure. There is a considerable partitioning of the solute atoms on either site, with some elements preferring the site of high CN, the others the site of low CN, and follows both geometric and electronic criteria. Contrary to what is generally observed for these kinds of systems, DFT calculations fail in both reproducing lattice parameters and site occupancies. We have shown that this is due to an improper description of Mn atom in the frame of the PBE-DFT. This obviously has implications for all the literature calculations reporting energies and volumes of compound with this element.

Acknowledgements

The authors acknowledge Fabrice Couturas for help in the synthesis and characterization of the samples, Eric Leroy for the microprobe analysis, Laetitia Laversenne from the ILL for the neutron diffraction measurements on D1B. DFT calculations were performed using HPC resources from

GENCI–CINES (Grant A0060906175). JCC thanks the Vienna researchers, Georg Kresse for the fruitful exchange and Fabien Tran for his patience in testing the anomalies in the β-Mn volume.

References

[1] A.J. Bradley, J. Thewlis, The crystal structure of α-manganese, Proc. R. Soc. (London) A115 (1927) 459-471, https://doi.org/10.1098/rspa.1927.0103.
[2] J.-M. Joubert, M. Phejar, The crystal chemistry of the χ phase, Prog. Mater. Sci. 54(7) (2009) 945-980, https://doi.org/10.1016/j.pmatsci.2009.04.002.
[3] C.B. Shoemaker, D.P. Shoemaker, T.E. Hopkins, S. Yindepit, Refinement of the structure of β-manganese and of a related phase in the Mn-Ni-Si system, Acta Crystallogr. B34 (1978) 3573-3576, https://doi.org/10.1107/S0567740878011620.
[4] O.B. Karlsen, A. Kjekshus, C. Romming, E. Rost, The crystal structure of the low-temperature $Au_{80-v}Cu_vSn_{20}$, Acta Chem. Scand. 46 (1992) 1076-1082, https://doi.org/10.3891/acta.chem.scand.46-1076.
[5] W. Xie, S. Thimmayah, J. Lamsal, J. Liu, T.W. Heitmann, D. Quirinale, A.I. Goldman, V. Pecharsky, G.J. Miller, β-Mn-type $Co_{8+x}Zn_{12-x}$ as a defect cubic Laves phase: site preferences, magnetism, and electronic structure, Inorg. Chem. 52 (2013) 9399-9408, https://dx.doi.org/10.1021/ic4009653.
[6] U. Burkhardt, A. Winkelmann, H. Borrmann, A. Dumitriu, M. König, G. Cios, Y. Grin, Assignment of enantiomorphs for the chiral allotrope β-Mn by diffraction methods, Science Advances 7 (2021) eabg0868, https://dx.doii.org/10.1126/sciadv.abg0868.
[7] R. Pöttgen, V. Hlukhyy, A. Baranov, Y. Grin, Crystal structure and chemical bonding of Mg_3Ru_2, Inorg. Chem. 47 (2008) 6051-6055, https://doi.org/10.1021/ic800387a.
[8] K. Schubert, T.R. Anantharaman, H.O.K. Ata, H.G. Meissner, M. Pötzschke, W. Rossteutscher, E. Stolz, Einige strukturelle Ergebnisse an metallischen Phasen (6), Naturwissenschaften 47(22) (1960) 512-512, https://doi.org/10.1007/BF00641115.
[9] P. Riani, K. Sufryd, G. Cacciamani, About the Al–Cu–Si isothermal section at 500°C and the stability of the ε-$Cu_{15}Si_4$ phase, Intermetallics 17 (2009) 154-164, https://dx.doi.org/10.1016/j.intermet.2008.10.011.
[10] T. Nakajima, K. Karube, Y. Ishikawa, M. Yonemura, N. Reynolds, J.S. White, H.M. Ronnow, A. Kikkawa, Y. Tokunaga, Y. Taguchi, Y. Tokura, T. Arima, Correlation between site occupancies and spin-glass transition in skyrmion host $Co_{10-x/2}Zn_{10-x/2}Mn_x$, Phys. Rev. B 100 (2019) 064407, https://doi.org/10.1103/PhysRevB.100.064407.
[11] H. Büchler, K.-J. Range, Zur Kenntnis des β-Mangan-Typs: Hochdrucksynthese und Strukturverfeinnerung von $AlAu_4$, J. Less-Common Met. 161 (1990) 347-354, https://doi.org/10.1016/0022-5088(90)90047-N.
[12] H.J. Goldschmidt, Occurrence of the β-manganese structure in transition metal alloys, and some observations on χ-phase equilibria, Acta Crystallogr. 10 (1957) 769, https://doi.org/10.1107/S0365110X57002649.
[13] D.A. Evans, K.H. Jack, Interstitial alloys with the structure of β-manganese, Acta Crystallogr. 10 (1957) 769-770, https://doi.org/10.1107/S0365110X57002649.
[14] W. Jeitschko, H. Nowotny, F. Benesovsky, Ein Beitrag zum Dreistoff: Molybdän-Aluminium-Kohlenstoff, Monatsh. Chem. 94(1) (1963) 247-251, https://doi.org/10.1007/BF00900244.
[15] W. Jeitschko, H. Nowotny, F. Benesovsky, Phasen mit aufgefüllter β-Manganstruktur, Monatsh. Chem. 95(4-5) (1964) 1212-1218, https://doi.org/10.1007/BF00904716.
[16] J.R. Stewart, R. Cywinski, Real-time kinetic neutron powder diffraction study of the phase transition from alpha-Mn to beta-Mn, J. Phys., Condens. Matter. 11(37) (1999) 7095-7102, https://doi.org/10.1088/0953-8984/11/37/307.
[17] T. Yamada, N. Kunitomi, Y. Nakai, D.E. Cox, G. Shirane, Magnetic structure of α-Mn, J. Phys. Soc. Jpn. 28(3) (1970) 615-627, https://doi.org/10.1143/JPSJ.28.615.

[18] J. Hafner, D. Hobbs, Understanding the complex metallic element Mn. II. Geometric frustrations in β-Mn, phase stability, and phase transitions, Phys. Rev. B68 (2003) 014408, https://doi.org/10.1103/PhysRevB.68.014408.
[19] M. Mekata, Y. Nakahashi, T. Yamaoka, Magnetic properties of α and β manganese containing 1 at.% transition metals, J. Phys. Soc. Jpn. 37(6) (1974) 1509-1511, https://doi.org/10.1143/JPSJ.37.1509.
[20] T. Hori, Antiferromagnetism of β-Mn alloys containing cobalt, J. Phys. Soc. Jpn. 38 (1975) 1780, https://doi.org/10.1143/JPSJ.38.1780.
[21] S. Akimoto, T. Kohara, K. Asayama, Nuclear magnetic relaxation in β-Mn alloys, Solid State Commun. 16 (1975) 1227-1229, https://doi.org/10.1016/0038-1098(75)90152-0.
[22] Y. Nishihara, S. Ogawa, S. Waki, Mössbauer study of β-Mn alloys with iron and tin - weak itinerant-electron antiferromagnetism of β-Mn alloys, J. Phys. Soc. Jpn. 42(3) (1977) 845-852, https://doi.org/10.1143/JPSJ.42.845.
[23] M. Katayama, K. Asayama, Hyperfine field in weakly antiferromagnetic β-Mn alloys, J. Phys. Soc. Jpn. 44(2) (1978) 425-432, https://doi.org/10.1143/JPSJ.44.425.
[24] R. Yamauchi, M. Miyakawa, K. Sasao, K. Fukamichi, X-ray diffraction and magnetic properties of β-$Mn_{1-x}Os_x$ alloys, J. Alloys Compd. 311 (2000) 124-129, https://doi.org/10.1016/S0925-8388(00)01090-2.
[25] J.F. Drain, R. Drautz, D.G. Pettifor, Magnetic analytic bond-order potential for modeling the different phases of Mn at zero Kelvin, Phys. Rev. B89 (2014) 134102, https://doi.org/10.1103/PhysRevB.89.134102.
[26] P. Villars, Pauling File Binary Edition (on CD-rom), Version 1.0, ASM International2002.
[27] M. Miyakawa, R.Y. Umetsu, K. Sasao, K. Fukamichi, Antiferromagnetism and low-temperature specific heat of β-$Mn_{1-x}Ir_x$ alloys, J. Phys.: Condens. Matter 15 (2003) 4605-4612, https://doi.org/10.1088/0953-8984/15/26/310.
[28] J.-M. Joubert, Crystal chemistry and Calphad modelling of the σ phase, Prog. Mater. Sci. 53 (2008) 528-583, https://doi.org/10.1016/j.pmatsci.2007.04.001.
[29] J.-M. Joubert, J.-C. Crivello, Description of terminal substitutional solid solutions using the sublattice model, Calphad: Comput. Coupling Phase Diagrams Thermochem. 67 (2019) 101685, https://doi.org/10.1016/j.calphad.2019.101685.
[30] H. Okamoto, Phase diagrams for binary alloys, Desk Handbook, ASM International2000.
[31] W.K.P. Hohenberg, Inhomogeneous electron gas, Phys. Rev. (1964) 864-871, https://doi.org/10.1103/PhysRev.136.B864.
[32] W. Kohn, L. Sham, Self-consistent equations including exchange and correlation effects, Phys. Rev. 140 (1965) A1133-1140, https://doi.org/10.1103/PhysRev.140.A1133.
[33] P.E. Blöchl, Projector augmented-wave method, Phys. Rev., B 50(24) (1994) 17953-17979, https://doi.org/10.1103/PhysRevB.50.17953.
[34] G. Kresse, J. Furthmüller, Efficient iterative schemes for ab initio total-energy calculations using a plane-wave basis set, Phys. Rev., B 54 (1996) 11169-11186, https://doi.org/10.1103/PhysRevB.54.11169.
[35] G. Kresse, J. Hafner, Ab initio molecular dynamics for open-shell transition metals, Phys. Rev., B 48 (1993) 13115, https://doi.org/10.1103/PhysRevB.48.13115.
[36] G. Kresse, D. Joubert, From ultrasoft pseudopotentials to the projector augmented-wave method, Phys. Rev., B 59(3) (1999) 1758-1775, https://doi.org/10.1103/PhysRevB.59.1758.
[37] M. Ropo, K. Kokko, L. Vitos, Assessing the Perdew-Burke-Ernzerhof exchange-correlation density functional revised for metallic bulk and surface systems, Phys. Rev., B B77 (2008) 195445, https://doi.org/10.1103/PhysRevB.77.195445.
[38] J.P. Perdew, K. Burke, M. Ernzerhof, Generalized gradient approximation made simple, Phys. Rev. Lett. 77(18) (1996) 3865-3868, https://doi.org/10.1103/PhysRevLett.77.3865.

[39] J.P. Perdew, K. Burke, M. Ernzerhof, ERRATA: Generalized gradient approximation made simple [Phys. Rev. Lett. 77, 3865 (1996)], Phys. Rev. Lett. 78(7) (1997) 1396, https://doi.org/10.1103/PhysRevLett.78.1396.
[40] P.E. Blöchl, O. Jepsen, O.K. Andersen, Improved tetrahedron method for Brillouin-zone integrations, Phys. Rev., B 49 (1994) 16223-16233, https://doi.org/10.1103/PhysRevB.49.16223.
[41] H.J. Monkhorst, J.D. Pack, Special points for Brillouin-zone integrations, Phys. Rev., B 13 (1976) 5188-5192, https://doi.org/10.1103/PhysRevB.13.5188.
[42] R.F.W. Bader, Atoms in molecules. A quantum theory, Oxford University Press1990.
[43] G. Henkelman, A. Arnaldsson, H. Jónsson, A fast and robust algorithm for Bader decomposition of charge density, Comput. Mater. Sci. 36 (2006) 354-360, https://doi.org/10.1016/j.commatsci.2005.04.010.
[44] R. Nesper, Bonding patterns in intermetallic compounds, Angew. Chem. Int. Ed. 30 (1991) 789-817, https://doi.org/10.1002/anie.199107891.
[45] T. Kohara, K. Asayama, NMR study of anti-ferromagnetic β-Mn alloys, J. Phys. Soc. Jpn. 37(2) (1974) 401-407, https://doi.org/10.1143/jpsj.37.401.
[46] T. Shinkoda, K.-I. Kumagai, K. Asayama, Effect of spin fluctuations on the specific heat in βMn metal and alloys, J. Phys. Soc. Jpn. 46(6) (1979) 1754-1758, https://doi.org/10.1143/JPSJ.46.1754.
[47] J.R. Stewart, R. Cywinski, Nuclear and magnetic short-range order in some dilute β-Mn alloys, J. Magn. Magn. Mater. 272-276 (2004) 676-678, https://doi.org/10.1016/j.jmmm.2003.12.720.
[48] R. Zhang, Z. Gercsi, M. Venkatesan, A. Jha, P. Stamenov, J.M.D. Coey, Spin liquids and spin glasses in Mn-based alloys with the cubic A13 (βMn) structure, J. Magn. Magn. Mater. 501 (2020) 166429, https://doi.org/10.1016/j.jmmm.2020.166429.
[49] J.S. Kasper, B.W. Roberts, Antiferromagnetic structure of α-manganese and a magnetic structure study of β-manganese, Phys. Rev. 101(2) (1956) 537-544, https://doi.org/10.1103/PhysRev.101.537.
[50] R. Kohlhaas, W.D. Weiss, Magnetische Suszeptibilität des Mangans zwischen Helium-Temperatur und 2000 °K, Z. Nat.forsch. 24a (1969) 287-288, https://doi.org/10.1515/zna-1969-0220.
[51] H. Nakamura, K. Yoshimoto, M. Shiga, M. Nishi, K. Kakurai, Strong antiferromagnetic spin fluctuations and the quantum spin-liquid state in geometrically frustrated beta-Mn, and the transition to a spin-glass state caused by non-magnetic impurity, J. Phys., Condens. Matter. 9(22) (1997) 4701-4728, https://doi.org/10.1088/0953-8984/9/22/022.
[52] J.R. Stewart, R. Cywinski, μSR evidence for the spin-liquid-to-spin-glass transition in β-$Mn_{1-x}Al_x$, Phys. Rev. B59(6) (1999) 4305-4313, https://doi.org/10.1103/PhysRevB.59.4305.
[53] M. Shiga, H. Nakamura, M. Nishi, K. Kakurai, Damping of spin fluctuations of β-Mn by a nonmagnetic impurity: neutron and NMR studies, J. Magn. Magn. Mater. 140-144 (2009) 2009-2010, https://doi.org/10.1016/0304-8853(94)01071-4.
[54] J.R. Stewart, K.H. Andersen, R. Cywinski, Neutron polarization analysis study of the frustrated magnetic ground state of β-$Mn_{1-x}Al_x$, Phys. Rev. B78 (2008) 014428, https://doi.org/10.1103/PhysRevB.78.014428.
[55] H. Oyamatsu, Y. Nakai, N. Kunitomi, Impurity distribution on the sites of β-Mn structure for Mn(Co), Mn(Fe) and Mn(Ni) alloys, J. Phys. Soc. Jpn. 58(10) (1989) 3606-3615, https://doi.org/10.1143/JPSJ.58.3606.
[56] O.B. Karlsen, A. Kjekshus, H. Fjellvåg, P. Ravindran, R. Vidya, B.C. Hauback, Structure and magnetism of the β-Mn-Co solid-solution phase, J. Alloys Compd. 476 (2009) 9-13, https://doi.org/10.1016/j.jallcom.2008.09.011.
[57] J.R. Stewart, R. Cywinski, Magnetic short-range order in β $Mn_{1-x}Co_x$, J. Phys.: Condens. Matter 21 (2009) 124216, https://doi.org/10.1088/0953-8984/21/12/124216.
[58] C.W. Kimball, J.K. Tison, M.V. Nevitt, Hyperfine interactions at ^{57}Fe nuclei in intermetallic compounds of the Fe-Mn system with the β-manganese structure, J. Appl. Phys. 38(3) (1967) 1153-1154, https://doi.org/10.1063/1.1709521.

[59] A.S. Ilyushin, A.A. Katsnel'son, I.A. Nikanorova, Distribution of iron atoms in Fe-Mn alloys with the structure of β-Mn, Soviet Physics Journal 24 (1981) 278-281, https://doi.org/10.1007/BF00891608.
[60] A.S. Vinogradova, A.S. Ilyushin, I.A. Nikanorova, V.S. Rusakov, Mössbauer studies of the atomic distributions and hyperfine interactions in Mn-Fe alloys with β-Mn structure, Phys. Solid State 39(8) (1997) 1276-1280, https://doi.org/10.1134/1.1130060.
[61] J.R. Stewart, A.D. Hillier, J.M. Hillier, R. Cywinski, Structural and dynamical study of moment localization in β-$Mn_{1-x}In_x$, Phys. Rev. B82 (2010) 144439, https://doi.org/10.1103/PhysRevB.82.144439.
[62] M. Miyakawa, R.Y. Umetsu, K. Fukamichi, Specific heat and thermal expansion characteristics related to spin fluctuations in antiferromagnetic β-MnOs alloys, J. Phys.: Condens. Matter 13 (2001) 3809-3816, https://doi.org/10.1088/0953-8984/13/17/301.
[63] T. Hama, M. Matsumura, H. Yamagata, M. Miyakawa, R. Umetsu, K. Fukamichi, ^{55}Mn NMR/NQR study in β-MnOs alloys, J. Magn. Magn. Mater. 272-276 (2004) 503-504, https://doi.org/10.1016/j.jmmm.2003.12.389.
[64] M. Miyakawa, R.Y. Umetsu, M. Ohta, A. Fujita, K. Fukamichi, T. Hori, Spin fluctuation, thermal expansion anomaly, and pressure effects on the Néel temperature of β-MnM (M=Ru, Os, and Ir) alloys, Phys. Rev. B72 (2005) 054420, https://doi.org/10.1103/PhysRevB.72.054420.
[65] K. Sasao, R.Y. Umetsu, K. Fukamichi, Atomic site preference, the Néel temperature and specific heat of β-$Mn_{1-x}Ru_x$ alloys, J. Alloys Compd. 325 (2001) 24-28, https://doi.org/10.1016/S0925-8388(01)01270-1.
[66] C.J. Leavey, J.R. Stewart, B.D. Bainford, A.D. Hillier, Magnetic ground states and spin dynamics of β-$Mn_{1-x}Ru_x$ alloys, J. Phys.: Condens. Matter 19 (2007) 145288, https://doi.org/10.1088/0953-8984/19/14/145288.
[67] B.D. Rainford, J.R. Stewart, C.J. Leavey, A.D. Hilier, μSR study of the onset of magnetic order in β-Mn-Ru alloys, J. Magn. Magn. Mater. 310 (2007) 1314-1315, https://doi.org/10.1016/j.jmmm.2006.10.480.
[68] J.R. Stewart, A.S. Wills, C.J. Leavey, B.D. Rainford, C. Ritter, The magnetic structure of β-MnRu, J. Phys.: Condens. Matter 19 (2007) 145291, https://doi.org/10.1088/0953-8984/19/14/145291.
[69] C.W. Kimball, L.R. Sill, Mössbauer and susceptibility investigation of manganese-tin alloys with the beta-manganese structure, Phys. Rev. B1(10) (1970) 3953-3955, https://doi.org/10.1103/PhysRevB.1.3953.
[70] J.B. Dunlop, J.M. Williams, J. Crangle, ^{119}Sn Mössbauer and neutron diffraction investigation of β Mn-Sn solid solution, Physica 86-88B (1977) 269-271, https://doi.org/10.1016/0378-4363(77)90310-2.
[71] Y. Nakai, Neutron-diffraction and mössbauer spectroscopic studies of β-Mn(Sn) alloys, J. Phys. Soc. Jpn. 63(2) (1994) 775-780, https://doi.org/10.1143/jpsj.63.775.
[72] D.P. Dinega, M.G. Bawendi, A solution-phase chemical approach to a new crystal structure of cobalt, Angew. Chem. Int. Ed. 38(12) (1999) 1788-1791, https://doi.org/10.1002/(SICI)1521-3773(19990614)38:12%3C1788::AID-ANIE1788%3E3.0.CO;2-2.
[73] B. Sundman, J. Ågren, A regular solution model for phases with several components and sublattices, suitable for computer applications, J. Phys. Chem. Solids 42 (1981) 297-301, https://doi.org/10.1016/0022-3697(81)90144-X.
[74] T. Hori, H. Shiraish, Y. Ishii, Magnetic properties of β-MnCoZn alloys, J. Magn. Magn. Mater. 310 (2007) 1820-1822, https://doi.org/10.1016/j.jmmm.2006.10.582.
[75] S. Bigdeli, M. Selleby, A thermodynamic assessment of the binary Fe-Mn system for the third generation of Calphad databases, Calphad 64 (2019) 185-195, https://doi.org/10.1016/j.calphad.2018.11.011.
[76] B. Lindahl, M. Selleby, The Al-Fe-Mn system revisited - an updated thermodynamic description using the most recent binaries, Calphad: Comput. Coupling Phase Diagrams Thermochem. 43 (2013) 86-93, https://doi.org/10.1016/j.calphad.2013.05.001.

[77] W. Zheng, H. Mao, X.-G. Lu, Y. He, L. Li, M. Selleby, J. Ågren, Thermodynamic investigation of the Al-Fe-Mn system over the whole composition and wide temperature ranges, J. Alloys Compd. 742 (2018) 1046-1057, https://doi.org/10.1016/j.jallcom.2018.01.291.
[78] A. Walnsch, M.J. Kriegel, O. Fabrichnaya, A. Leineweber, Thermodynamic assessment and experimental investigation of the systems Al-Fe-Mn and Al-Fe-Mn-Ni, Calphad 66 (2019) 101621, https://doi.org/10.1016/j.calphad.2019.04.006.
[79] S. Dash, A.V. Lukoyanov, Nancy, D. Mishra, U.P. Mohamed Rasi, R.B. Gangineni, M. Vasundhara, A.K. Patra, Structural stability and magnetic properties of Mn_2FeAl alloy with a β-Mn structure, J. Magn. Magn. Mater. 513 (2020) 167205, https://doi.org/10.1016/j.jmmm.2020.167205.
[80] A. Walnsch, A. Leineweber, M.J. Kriegel, A third generation CaPhaD assessment of the Fe-Mn-Ti system part I: the binary subsystems Fe-Mn, Fe-Ti and Mn-Ti, Calphad: Comput. Coupling Phase Diagrams Thermochem. 81 (2023) 102555, https://doi.org/10.1016/j.calphad.2023.102555.
[81] A. Walnsch, A. Leineweber, M.J. Kriegel, A third generation CalPhaD assessment of the Fe-Mn-Ti system part II: the ternary system Fe-Mn-Ti, Calphad: Comput. Coupling Phase Diagrams Thermochem. 81 (2023) 102553, https://doi.org/10.1016/j.calphad.2023.102553.